Practical implementation of a single-qubit rotation algorithm

Christoffer Hindlycke* and Jan-Åke Larsson[†]
Department of Electrical Engineering, Linköping University 581 83 Linköping, SWEDEN
(Dated: October 30, 2024)

The Toffoli is an important universal quantum gate, and will alongside the Clifford gates be available in future Fault-Tolerant Quantum Computing hardware. Many quantum algorithms rely on performing arbitrarily small single-qubit rotations for their function, and these rotations may also be used to construct any unitary from a limited (but universal) gate set; it is then of significant interest how to carry out such rotations. In this work, we evaluate the performance of a recently proposed single-qubit rotation algorithm using the Clifford+Toffoli gate set by implementation of a one-shot version on both a real and simulated quantum computer. We test the algorithm under various simulated noise levels utilizing a per-qubit depolarizing error noise model, finding that the errors are seemingly explained by a binomial distribution wherein these errors change controlling ancilla measurements from 0 into 1. Similar observations appear to hold when conducting live runs; noise levels here make further meaningful conclusions difficult, although for the smallest possible number of ancillary controls n we do note that error mitigation is helpful. Our results suggest that the algorithm will perform well under up to 1% noise, under the noise model we chose. We further posit the use of our algorithm as a benchmark for Quantum Processing Units, given that its one-shot version has a very modest (in fact close to minimal) linear increase in total number of qubits and Toffoli gates required when increasing n: We provide details on how to go about this.

I. INTRODUCTION

The Toffoli gate is instrumental for quantum computing, being an indispensable part of for example Shor's algorithm [1, 2], quantum error correction [3–8], and shallow quantum circuits [9]. Many of these quantum algorithms also require arbitrarily small single-qubit rotations, making approximation of generic gates using a finite gate set essential. This is especially true in the Fault Tolerant Quantum Computing (FTQC) era where direct fault-tolerant constructions are typically available only for a limited number of gates, so that short generation of generic gates is necessary for high performance computing [10].

The Clifford+Toffoli gate set will be available in future quantum computer hardware: It is therefore natural to ask if generic unitaries can be built using that gate set, and indeed, if they can be built efficiently and explicitly. We were recently able to answer this question in the affirmative, by giving an explicit construction for approximating any z-axis rotation to within distance ϵ using the Clifford+Toffoli gate set with expected Toffoli count $4\lceil \log \frac{1}{\epsilon} \rceil$, see Ref. [11]: Three such rotations allows approximation of any single qubit gate. Our construction is simple and efficient, requiring only a trigonometric expression of the desired rotation angle, rounded to the desired accuracy. The resulting algorithm succeeds in applying a rotation ϵ -close to that desired with probability strictly greater than 1/2, has expected gate depth $4\lceil\log\frac{1}{\epsilon}\rceil+6$ and uses $2\lceil\log\frac{1}{\epsilon}\rceil$ ancillas. Should the rotation not be applied, a Z gate is applied instead, and ancilla measurements indicate this.

In this work, we put our single-qubit rotation algorithm through practical testing using IBM's Qiskit software suite [12]: We provide explicit circuits implementing a one-shot version of the algorithm for varying numbers of ancillary controls n, then run these circuits on both real and simulated quantum computers. We apply quantum tomography to categorize the unitaries these circuits actually implement, and compare them to their theoretical counterparts: Full experimental details and results are made available.

Beyond its usefulness in an FTQC device, our algorithm also demonstrates a linear scaling in its requisite number of ancilla and Toffoli gates. This paves the way for it to be used as a remarkably simple means of benchmarking for comparing Noisy Intermediate Scale Quantum (NISQ) devices: The number of qubits in active use along with number of universal gates are typically considered the greatest contributors of noise within such a device [10]. Typically our algorithm is utilized by first selecting a tolerable error rate ϵ which decides the number of ancillary controls n; here one then chooses the smallest such n. There is, however, nothing preventing a reversed means of application: Select first an n disregarding error considerations, which then dictates the ϵ . In so doing, the total number of qubits in active use by the algorithm will be set to 2n-2, plus a single qubit as target for the rotation, and the total number of required Toffolis will also be 2n-2. In other words, increasing n by 1 increases total number of qubits and Toffolis by 2 each. The actual benchmarking can then consist of observing the actual probability of the rotation being applied as compared to its theoretical value, or reconstructing the noisy channel via quantum state [13] and process [14] tomography and comparing it against a suitable unitary, or both of these in tandem: We provide an example of how to go about the latter by explicit implementation in this

^{*} christoffer.hindlycke@liu.se

[†] jan-ake.larsson@liu.se

work.

The rest of this article is structured as follows. We first provide a brief description of the single-qubit rotation algorithm of Ref. [11]. We then describe a number of circuit simplifications possible, several of which are new. Next, we go into detail on our experimental setup, describing how quantum state and process tomography allows us to analyze the effect of the quantum channel realized by our (noisy) quantum circuit. This is followed by a presentation of our results, and some discussion. Throughout this work, we assume a working knowledge of discrete quantum computation, to which a comprehensive introduction may be found in Ref. [15].

II. THE SINGLE-QUBIT ROTATION ALGORITHM

We briefly describe the algorithm implemented in this work; for more details, we refer to Ref. [11]. Let R_{θ} denote a single-qubit rotation (along the z-axis) of angle θ radians. A simple example taken from [15, p. 198], of a circuit implementing the rotation $R_{\arccos 3/5}$, can be found in Figure 1a. This circuit can then be generalized as depicted in Figure 1b. Another way of looking at the circuit in Figure 1a is that it performs a comparison with the classical constant k=3. Increasing the number of ancillary controls n then allows us to set other k: Say that we wish to apply a specific rotation of angle θ to within distance ϵ . Then by Theorem 1 of Ref. [11], we should choose a number of ancillary controls equal to the (smallest) integer n such that

$$n \ge 1 + \left\lceil \log \frac{1}{\epsilon} \right\rceil,\tag{1}$$

this in turn yields a comparison constant

$$k = 2^{n-1} + \left[2^{n-1} \tan \frac{\theta}{2} + \frac{1}{2} \right].$$
 (2)

With n and k fixed we may construct a circuit carrying out a rotation R_{θ^*} , where we are guaranteed that

$$||R_{\theta} - R_{\theta^*}|| \le |\theta - \theta^*| \le \epsilon, \tag{3}$$

see Figure 1b for the circuit in question.

The $\geq k$ tests admit efficient explicit constructions found in Ref. [11]; in addition, we have provided the circuits we use, see Appendix A. The circuit in Figure 1b works by marking k states using the S gate, and once these states are so marked, one can show that the circuit either applies the rotation R_{θ^*} with probability strictly greater than 1/2, or failing that, a Z gate. If R_{θ^*} was applied, this is heralded by all ancillary controls measuring 0: The circuit may then be used in a repeat-until-success algorithm, if so desired. In this work, we use a one-shot version of the algorithm; see the chapter on experimental setup.

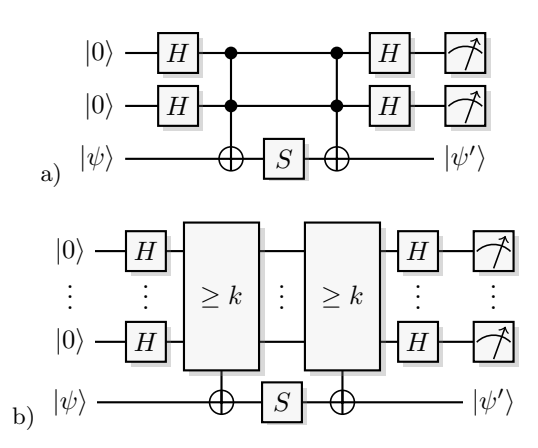


FIG. 1. Circuits for approximate single-qubit rotation. a) Circuit that applies R_{φ} to $|\psi\rangle$ (cos $\varphi=3/5$, sin $\varphi=4/5$) with probability 5/8; otherwise a Z gate. b) Circuit that applies R_{θ^*} to $|\psi\rangle$, ϵ -close to a desired rotation R_{θ} with high probability, where number of ancillary controls n and comparison constant k should be chosen as in Equations 1, 2.

III. CIRCUIT SIMPLIFICATIONS

The circuit in Ref. [11] comes with several simplifications already enacted; we describe these simplifications here in the interest of thoroughness, then add a few new ones. Before doing so, we divide the ancilla used by the circuit into outer and inner ancilla. Outer ancilla refers to those measured at the end of the circuit. Inner ancilla denotes those internal to the $\geq k$ test.

The original comparator construction of Ref. [11] performs a bit-wise > k test of the external ancilla against a classical constant k using a ripple-carry comparator with carry-in; turning this into a $\geq k$ test then entails setting the carry-in to 1. Subroutines implementing quantum bit-comparisons with carry-in that compare against 0 (a quantum OR gate or a Toffoli with inverted controls and inverted output) and 1 (a quantum AND gate, that is a Toffoli) can be found in Ref. [11] together with simplifications for constant carry-in 1: Below we assume familiarity with these. The first simplification then consists of reducing k (and thereby n). As long as the least significant bit of k is 0, the first comparison will check if the input bit is greater than or equal to 0, and so always outputs 1 for true. We can then remove that bit from k and keep the carry-in of 1. Since we are then effectively dividing k by 2, this also means we reduce n by 1: this happens if k is even. This simplification shows that increasing nis not always beneficial, in that different n may end up giving the same precision.

After the above, the first comparison will always be against the bit 1, so the comparison becomes a CNOT from the first outer ancilla; we may then simply skip the comparison and use the first outer ancilla as the first control in the second comparison. The last comparison outputs the result, and so uses the qubit to be rotated as its target.

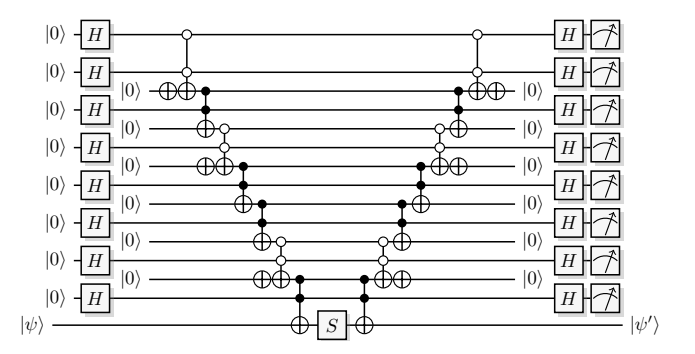
More crucially, since our algorithm applies the $\geq k$ test twice, once before and once after applying an S gate to the target, we may omit the uncomputation part on the first application, and also omit the (forward) computation part on the second application by re-using the internal ancilla, which results in halving the number of Toffolis required.

And now we add more simplifications. The first such depends on whether we have native access to an OR gate (Toffoli with inverted controls and inverted target) or not. If not, we may simplify as follows. Following the above, the least significant bit of k will always be 1, but other bits may be 0; if so, we invert the controls of the Toffoli by adding X gates. The reason we are not inverting the target is that X commutes with Toffoli on the target (a fact which we exploit below): Hence an X to the right and left of the target cancel each other out, as $X^2 = I$. Since we are dividing our $\geq k$ test into a computation and uncomputation part, the X gates to the right of the computation Toffoli and to the left of the uncomputation Toffoli again cancel each other out, and so may be omitted.

Additionally, there is no need to return the internal ancillas to the state $|0\rangle$; they must simply be returned to a known state. We may then also omit the X gates to the right of the uncomputation Toffoli. Also, if we have an X on the target both before and after a Toffoli, they cancel out by the reasoning above: This occurs only if the corresponding bit values of k sum to 0 mod 2. If they do not, it means we have one normal and one inverted control for the same internal ancilla, and so the X count is 1. Note also that $|+\rangle$ is invariant under X: Whenever an external ancilla is a control for a Toffoli, that control need not be inverted.

Finally, when using a quantum computer to run our algorithm, typically a state preparation scheme is available (and so it is in Qiskit). This further reduces the circuit complexity, as we may replace any X gates on internal ancilla with preparing the ancilla in the requisite state $|0\rangle$ or $|1\rangle$, and rather than applying an initial set of Hadamard gates to the external ancilla, we initialize them in the state $|+\rangle$. Some architectures may even have native support for measuring in different bases; if so, we may omit the final n Hadamard gates as well, and opt to measure in the Pauli X basis.

We exemplify in Figure 2 by comparing our algorithm approximating the T gate for n=8, before and after the additional simplifications described above: Here we manually switch basis before measuring. In this case, assuming we consider a Toffoli with inverted controls as using a total of four X gates, we were able to reduce the X count by 30, and the Hadamard count by 8. In general, for a reduced k and n, the X count reduces by $10\sum_i(k_i\oplus 1)$, and the Hadamard count reduces by n (2n if we can measure directly in Pauli X). This also reduces circuit depth considerably.



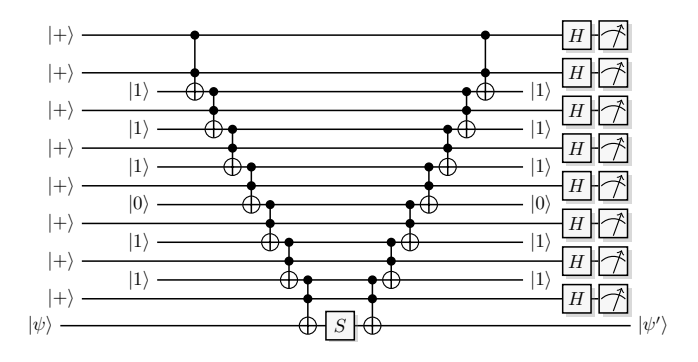


FIG. 2. Gate array that approximates the T gate to within $\epsilon < 2.6 \times 10^{-4}$, before and after simplifications, when performing manual basis switching prior to measurement; here $k = 181 = 10110101_2$.

IV. EXPERIMENTAL SETUP FOR A TOMOGRAPHIC EXPERIMENT

The intent behind our experiment is two-fold. Our primary concern is verifying theoretical predictions as to the behavior of our algorithm by comparing them to experimental outcomes. Also, we should like some estimation of our algorithm's performance under various noise levels.

To achieve this, we reconstruct the actual channel implemented by the algorithm using quantum tomography. There are two stages to this. In the first stage, quantum state tomography is applied to estimate the outcome when the channel our algorithm implements acts on a number of basis states [13]. In the second stage, these estimates are used to reconstruct the channel in question via quantum process tomography [14]. The reconstructed channel may then be compared to a target unitary. When the R_{θ^*} rotation was applied, we compare against the T gate: All circuits in this experiment were constructed (i.e. had comparison constant k deduced) using $\theta = \frac{\pi}{4}$. For this reason, we denote the R_{θ^*} rotation by T^* . The case of T^* not being applied shall be referred to as applying a Z^* rotation, in which case comparison is made against the Z gate. Our means of this comparison will be that of Process Fidelity (PF) [16].

The quantum process tomography of Ref. [14] requires (approximations of) the output state from the unknown channel acting on the basis states $|0\rangle$, $|1\rangle$, $|+\rangle$, $|+i\rangle$. Ap-

proximating this in turn requires preparing each of these states, applying the channel and then measuring each state in the three Pauli bases $X,\,Y,\,Z$. Hence, for a fixed number of external ancilla n we need a total of 12 circuits; each such circuit is run 10^5 times. For the simulated runs, in addition to perfect (error-free) runs, we also introduce a per-qubit depolarizing error occurring when applying a gate and measuring with probability 0.01, 0.05 and 0.1 (with the same error rate for gates and measuring). Error-free runs thus yield a unitary, while all other runs yield a channel.

For the live runs, in addition to running the circuits directly, error mitigation is also utilized in the form of (separately applied) dynamical decoupling and gate twirling. Dynamical decoupling [17] means adding Pauli gates, whose effect sum to the identity, to prevent qubits from sitting idle for too long: Since we use a ripple-carry comparator, it is indeed the case that most of our ancilla qubits are idle throughout the majority of the execution time. Owing to the technical implementation of Qiskit Quantum Processing Units (QPU), this may then help mitigate errors. Pauli twirling [18] entails adding Pauli gates before and after the gates of a circuit in such a way that the effect of each gate remains the same: The intent here is to transform the (unknown) noise of the channel into Pauli noise, which tends to accumulate slower [19]. Pauli twirling can be combined with error mitigation techniques specifically aimed at suppressing Pauli noise [19], though we have not done so here. Live runs were carried out using the Qiskit QPU ibm_nazca: simulated runs were carried out using Qiskit's AerSimulator.

While there exists a repeat-until-success version of the single-qubit rotation algorithm in Ref. [11], we have elected to use a one-shot version: This means number of repetitions is set to 1. We ran the algorithm for number of external ancilla $2 \le n \le 8$. n=2 is the lowest possible number of external ancilla and results in the original rotation circuit of Nielsen & Chuang [15]. As for n=3, this yields $k=6=110_2$, which in turn reduces to $k=4=11_2$ and hence n=2; this has been included in the plots as a point of reference.

As noted in Ref. [11], for the T gate n=8 yields a good theoretical (noise-less) precision roughly equal to 2.579×10^{-4} : One would need $n \ge 13$ to get a better result, and so we felt n=8 was a good stopping point. All rotation circuits used may be found in Appendix A.

All measurements were used to calculate observed probability of applying T^* . Based on whether T^* or Z^* was applied, measurements of the target qubit were then used to approximate the two unitaries using quantum state and process tomography; the output is two quantum channels that also contain noise. With these estimates in hand for a given n, we then calculated the PF [16] compared to the T gate (when T^* was applied) and the Z gate (when Z^* was applied).

V. RESULTS

Before discussing our results, we remark that Qiskit offers an implementation of the phase gate, that is we may freely apply any desired rotation along the z-axis. Utilizing such a gate is of course preferable (when available) rather than manually implementing a rotation.

We should also mention that Average Gate Fidelity (AGF) [16] is another common way of measuring how "close" two unitaries are to each other: Yet, AGF is an affine transformation of PF, and so we find that depicting the two (often nearly identical plots) alongside each other offers little merit. That said, both AGF and PF are available in the tables found in Appendix B, along with theoretical and observed probabilities of applying T^* .

This section will be divided into results for simulated and live runs.

A. Simulated runs

Let us first look at the probability of applying T^* , see Figure 3. We abbreviate the probability of a per-qubit depolarizing error as δ ; though somewhat difficult to tell from the plot, $\delta=0$ gives outcomes in excellent accordance with theoretical predictions. As expected given the increasing gate depth and number of measurements necessary as n increases, increasing δ leads to decreasing probability of success. Even so, at $\delta=0.01$, we still have probability (close to) 1/2 of applying T^* .

Comparing the theoretical predictions with the simulations at the different δ values we find that the latter are proportional to the ideal prediction, but with an additional exponential dependence on the number of ancillas n. For $n \geq 4$, the simulated curves at nonzero δ are all close to

$$P_{\delta}(0^n) = P_0(0^n)(1 - c_{\delta})^{n-1}, \tag{4}$$

see the dotted lines in Figure 3. The case n = 2 (and n=3) do not follow this pattern, one possible reason for this is that there are no ancillas internal to the comparator with k, which likely gives a different error propagation. Equation (4) suggests that the simulations behave as if all the errors change only controlling ancilla measurement outcomes from 0 into 1, independently with equal probability c_{δ} for each controlling ancilla. The values used in Figure 3 are $c_{0.01} = 0.02925$, $c_{0.05} = 0.13280$ and $c_{0.1} = 0.23788$, all of which are close to 3δ or actually closer to $3\delta(1-\delta)^2 + \delta^3$ (with values 0.02940, 0.13550, and 0.24400), the probability that a single qubit has three independent random errors with an odd number of inversions. These are only observations at this point and we have not been able to verify the nature of the underlying behavior. Unfortunately also the used simulation toolkit does not offer further insight here.

When the controlling ancilla are all 0 the circuit should have performed the T^* rotation. We use the PF to assess

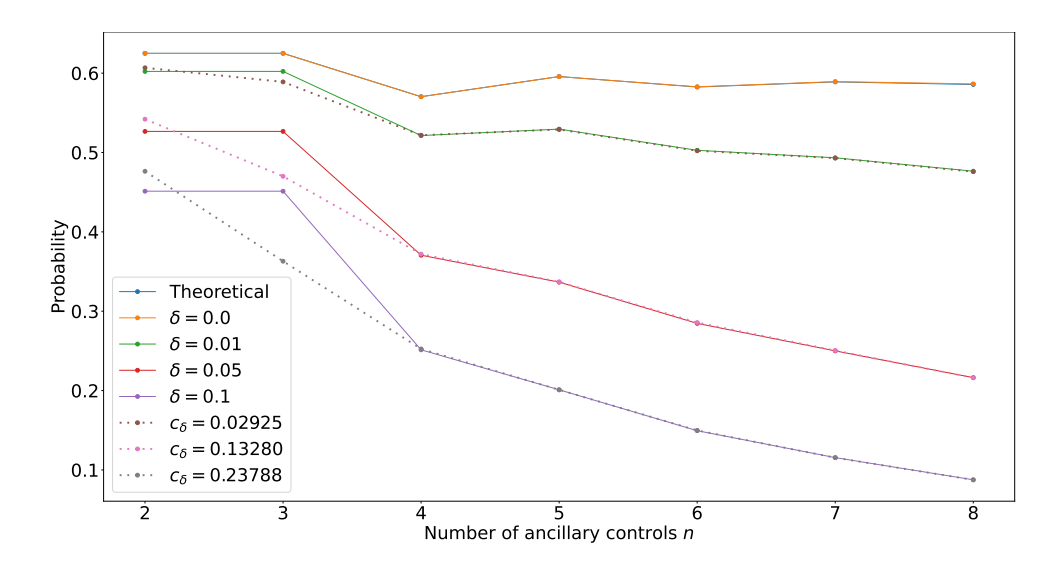


FIG. 3. Probability of applying T^* , simulated runs.

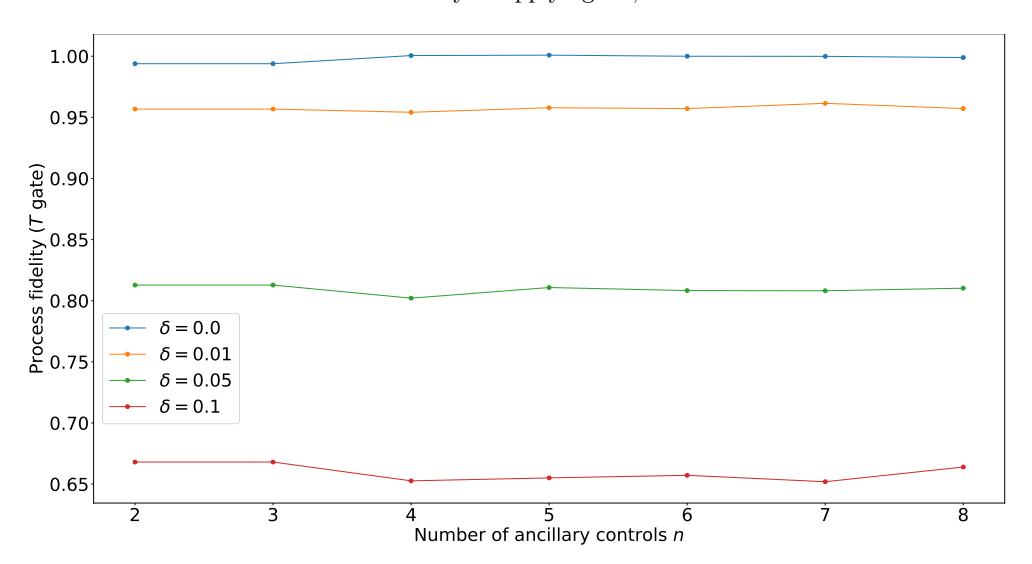


FIG. 4. PF calculated for T^* and T, simulated runs.

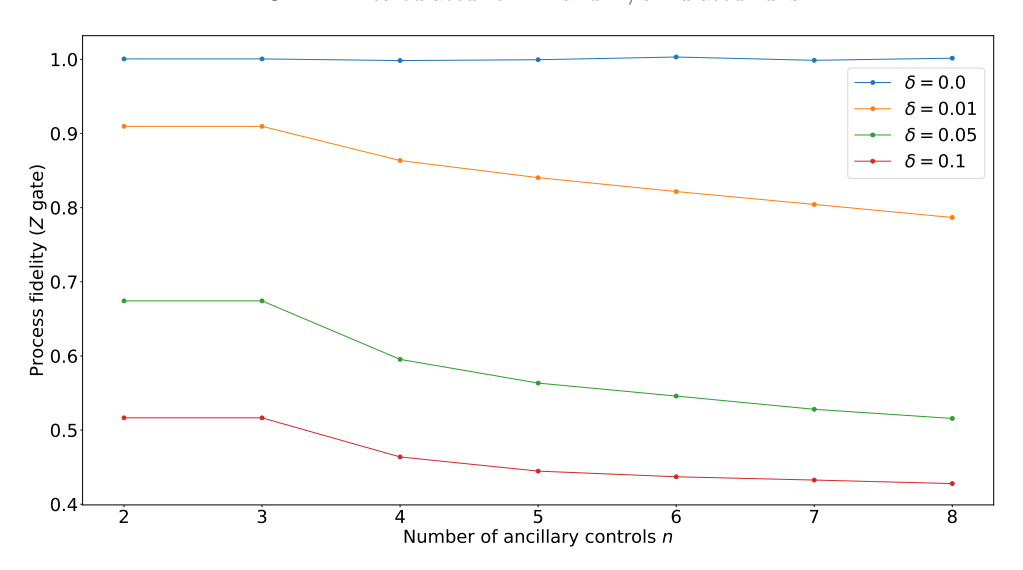


FIG. 5. PF calculated for Z^* and Z, simulated runs.

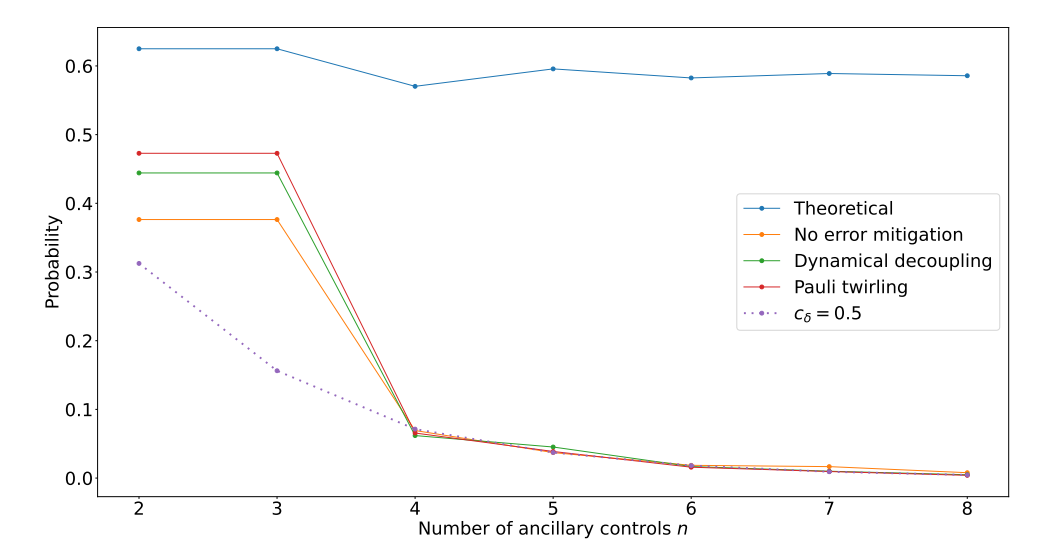


FIG. 6. Probability of applying T^* , live runs.

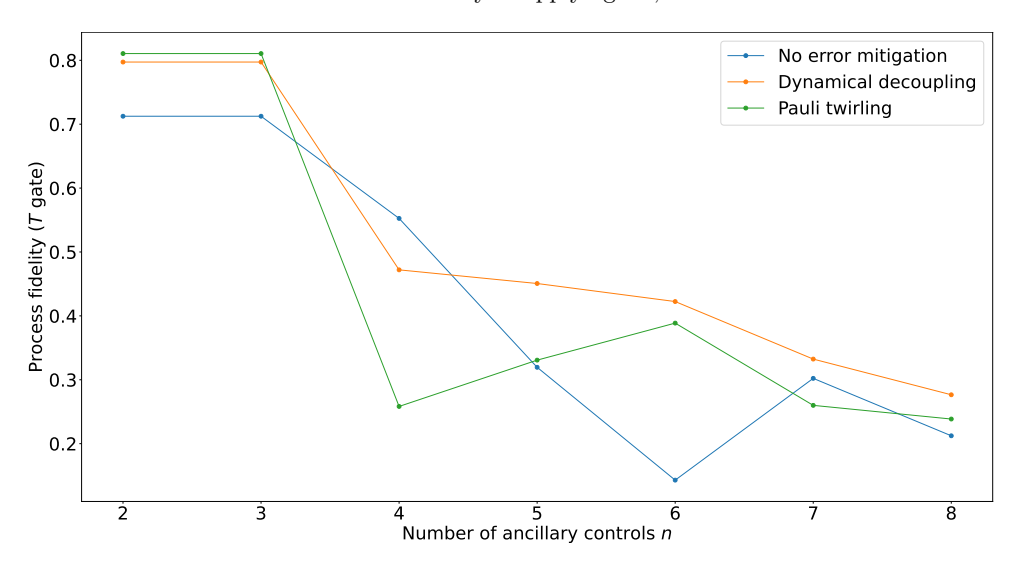


FIG. 7. PF calculated for T^* and T, live runs.

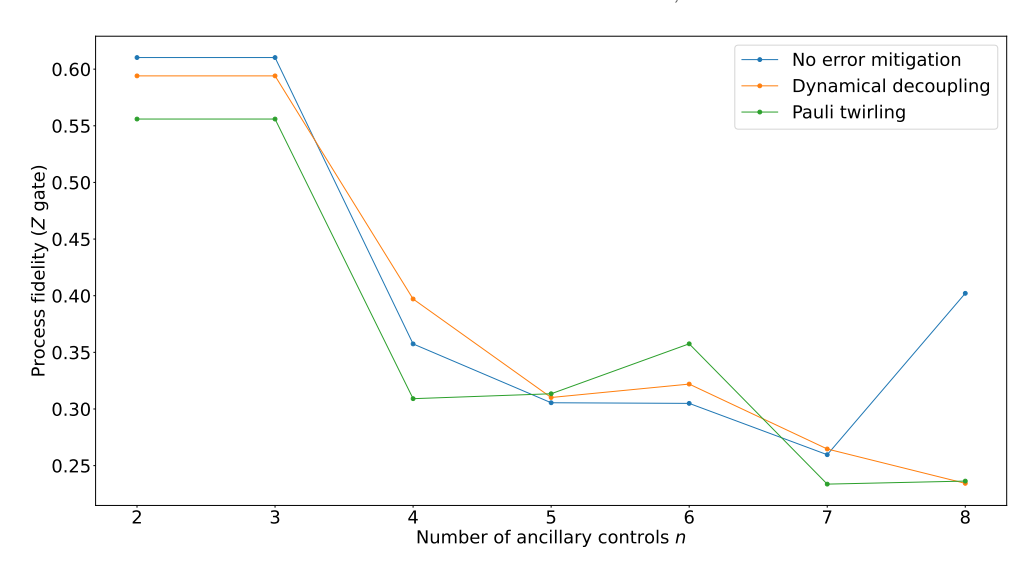


FIG. 8. PF calculated for Z^* and Z, live runs.

the quality of the rotation, to compare the actual noisy T^* to the desired T gate. The simulated PF can be found in Figure 4. We should point out that the angle error $|\theta-\theta^*|$ is 0.14190 at n=2 (and n=3) which may seem large in radians, but corresponds to an PF of $\frac{1}{2}+\frac{1}{2}\cos(\theta-\theta^*)=0.99497$. The increase for n=4 is just visible in the figure, the angle error is 0.06786 which corresponds to a PF of 0.99775, which is close enough to 1 to push the simulation output above 1 as seen in the PF table in Appendix B. When using the PF as figure of merit, there seems to be little to gain from increasing n; the benefit (if any) is only there for very low noise.

This can also be seen in the behavior for other values for δ : If the improvements were almost not visible before, they are now completely absent. Interestingly, the PF remains almost constant as we increase n, suggesting that larger values for δ only influences the "starting point" as it were. The reason is likely the already noted behavior, that the errors in the ancillary controls will give nonzero ancillary outcomes, so a failure rather than an erroneous rotation that would be counted as a successful rotation. The errors directly influencing the target will remain, and constitute the reason for the lowered starting point.

The PF plot for the failed runs, when one or more controlling ancilla outcomes are nonzero, show a slightly different behavior. In this case we compare the noisy Z^* to the ideal Z gate, as depicted in Figure 5. Again, $\delta=0$ gives simulation outcomes that align with theoretical predictions, but here for nonzero δ the PF does decrease slowly with increased n, the rate is also here exponential at about 1% to 1.5% decrease per step in n. The reason for the decreasing PF for Z^* is likely that errors in the controls, causing additional non-zero controlling ancilla measurement outcomes, contribute in this case unlike for T^* . Thus, we see errors both from the target and the controls in this case, meaning that an increased number of controls does increase the errors.

Given the propensity for gradually worsening PF between Z^* and Z, it might in the case of systems with more substantial error rates be advisable to stick to the present one-shot version of the algorithm, rather than the repeat-until-success version also found in Ref. [11], instead compensating by performing some post-selection procedure to retrieve valid measurements.

B. Live runs

See Figure 6 for the probability of applying T^* for live runs. Here, the situation is far from ideal. For n=2, error mitigation seems to have some effect, as we are seeing success probability on par with the simulation for $\delta = 0.1$. This is no longer the case for $n \geq 4$, as here we struggle to see any real difference in outcome regardless of error mitigation.

We have included a dotted plot for $P_{0.5}(0^n)$, which we note adheres admirably to the observed probabilities. This should not be taken as an attempt at classifying the

type of noise we are seeing: The likely noise in the actual QPU is far more complex than the depolarizing errors used in our simulations. An example of such is correlated noise [20]. Correlated noise would affect $n \geq 4$ much more than the short and relatively simple circuit for n=2, depicted in Figure 1a, and may offer a better explanation; we merely found it interesting we were able to get such a good fit using a simplified noise model, though perhaps this comes down to all observed probabilities decreasing exponentially.

The PF for the noisy T^* as compared to the T gate is as indicated in Figure 7. Also here, for n=2 the PF is on par or even slightly better than the simulation for $\delta=0.1$, especially when using error mitigation. For $n\geq 4$, as one might expect given the above discussion, noise levels are too high to draw meaningful conclusions. We get arguably similar results for PF when comparing Z^* to the Z gate, as evidenced by Figure 8: Again, noise levels prohibit fruitful analysis.

VI. CONCLUSIONS

We have devised an experimental implementation of a one-shot version of the single-qubit rotation algorithm described in Ref. [11], and carried out experimental runs on both simulated (at various noise levels) and real quantum computers using the Qiskit software suite [12]. We provide a full description of the simplifications of the circuit used in the single-qubit rotation algorithm, and introduce several additional ones: Reducing circuit depth and gate count is always useful in practical implementations.

Simulation outcomes are well in line with theoretical predictions, and suggest some simple patterns, which motivates further study. In the simulation we use the error model of depolarizing errors, this is a rather strong assumption; more generic noise like correlated noise may be a problem in our larger live-run examples.

Live run outcomes adhere less well to predictions: We provide conjecture on how to resolve this. Larger sample sizes seem an obvious improvement; given the noise levels seemingly present, improvements in quantum hardware would also be desirable. Noise reduction also seems crucial, we can think of a few ways to go about this. Circuit optimizations for each n based on the particular technical implementation of the QPU being used is one: This is done as a matter of course when transpiling, but higher optimization settings here may help (we opted for light optimization), or it may even be the case that manual optimization can help. There are also various noise reduction techniques that could be employed, such as those intended for dealing with Pauli noise [19] which could be combined with the Pauli twirling error mitigation [18].

Our algorithm does work under modest noise levels, though such (low) noise levels that are required seem not presently available: This is unfortunate but expected, as our algorithm is primarily intended for use on FTQC devices, rather than Noisy Intermediate Scale Quantum (NISQ) computational devices. Hopefully, our conjectured means of resolving this as stated above may improve our algorithm's performance on NISQ devices somewhat. This seems to us a good starting point if utilizing our algorithm as a benchmark: It may well be that some relatively simple additional error-mitigation techniques will allow for good results when n=4, at which point n=5 is the next step, etc. We would also note that even though technically the algorithm does reduce in complexity whenever k is even (recall the discussion on circuit simplifications previously), such a reduction is not mandated: We can construct the explicit circuit for any n, should we so desire. This might then offer a tantalizing alternative to going straight from n=2 to n=4in our example: Construct and run the circuit for n=3instead, and see if this indeed yields more favorable results compared to n = 4, by the means described above,

i.e. simple comparisons of the probability of applying a rotation in conjunction with quantum tomography.

VII. DATA AVAILABILITY

All experimental data is available on reasonable request made to the corresponding author.

VIII. ACKNOWLEDGMENTS

This work acknowledges support from the WACQT Quantum Technology Testbed operated by Chalmers Next Labs, which is funded by the Knut and Alice Wallenberg Foundation.

- [1] P. W. Shor, Algorithms for quantum computation: discrete logarithms and factoring, in *Proceedings 35th Annual Symposium on Foundations of Computer Science* (1994) pp. 124–134.
- [2] P. W. Shor, Polynomial-Time Algorithms for Prime Factorization and Discrete Logarithms on a Quantum Computer, SIAM Journal on Computing 26, 1484 (1997).
- [3] P. W. Shor, Scheme for reducing decoherence in quantum computer memory, Phys. Rev. A **52**, R2493 (1995).
- [4] D. G. Cory, M. D. Price, W. Maas, E. Knill, R. Laflamme, W. H. Zurek, T. F. Havel, and S. S. Somaroo, Experimental Quantum Error Correction, Physical Review Letters 81, 2152 (1998).
- [5] E. Knill, R. Laflamme, R. Martinez, and C. Negrevergne, Benchmarking Quantum Computers: The Five-Qubit Error Correcting Code, Physical Review Letters 86, 5811 (2001).
- [6] J. Chiaverini, D. Leibfried, T. Schaetz, M. D. Barrett, R. B. Blakestad, J. Britton, W. M. Itano, J. D. Jost, E. Knill, C. Langer, R. Ozeri, and D. J. Wineland, Realization of quantum error correction, Nature 432, 602 (2004).
- [7] M. D. Reed, L. DiCarlo, S. E. Nigg, L. Sun, L. Frunzio, S. M. Girvin, and R. J. Schoelkopf, Realization of three-qubit quantum error correction with superconducting circuits, Nature 482, 382 (2012).
- [8] D. Nigg, M. Müller, E. A. Martinez, P. Schindler, M. Hennrich, T. Monz, M. A. Martin-Delgado, and R. Blatt, Quantum computations on a topologically encoded qubit, Science 345, 302 (2014).
- [9] S. Bravyi, D. Gosset, and R. König, Quantum advantage with shallow circuits, Science 362, 308 (2018).
- [10] J. Preskill, Reliable quantum computers, Proceedings of the Royal Society of London. Series A: Mathematical, Physical and Engineering Sciences 454, 385 (1998).
- [11] C. Hindlycke and J.-A. Larsson, Single-qubit rotation algorithm with logarithmic Toffoli count and gate depth, Phys. Rev. Res. 6, 10.1103/PhysRevResearch.6.L042027 (2024).

- [12] A. Javadi-Abhari, M. Treinish, K. Krsulich, C. J. Wood, J. Lishman, J. Gacon, S. Martiel, P. D. Nation, L. S. Bishop, A. W. Cross, B. R. Johnson, and J. M. Gambetta, Quantum computing with qiskit (2024), arXiv:2405.08810 [quant-ph].
- [13] J. B. Altepeter, D. F. James, and P. G. Kwiat, 4 qubit quantum state tomography, in *Quantum State Estima*tion, edited by M. Paris and J. Řeháček (Springer Berlin Heidelberg, Berlin, Heidelberg, 2004) pp. 113–145.
- [14] I. L. Chuang and M. A. Nielsen, Prescription for experimental determination of the dynamics of a quantum black box, Journal of Modern Optics 44, 2455–2467 (1997).
- [15] M. A. Nielsen and I. L. Chuang, Quantum computation and quantum information, Vol. 10th Anniversary Edition (Cambridge University Press, 2010).
- [16] M. A. Nielsen, A simple formula for the average gate fidelity of a quantum dynamical operation, Physics Letters A 303, 249–252 (2002).
- [17] L. Viola, E. Knill, and S. Lloyd, Dynamical decoupling of open quantum systems, Physical Review Letters 82, 2417–2421 (1999).
- [18] C. H. Bennett, G. Brassard, S. Popescu, B. Schumacher, J. A. Smolin, and W. K. Wootters, Purification of noisy entanglement and faithful teleportation via noisy channels, Physical Review Letters 76, 722–725 (1996).
- [19] P. W. Shor, Fault-tolerant quantum computation (1997), arXiv:quant-ph/9605011 [quant-ph].
- [20] D. Aharonov, A. Kitaev, and J. Preskill, Fault-Tolerant Quantum Computation with Long-Range Correlated Noise, Physical Review Letters 96, 050504 (2006).

Appendix A: Qiskit circuits

Below are (pre-transpiling) circuits used in this work. Note that here, the target qubit is in state $|0\rangle$ and measurements are carried out in the Pauli Z basis; in addition during the experiment, input states $|1\rangle$, $|+\rangle$, $|+i\rangle$ and measurement bases Pauli X, Pauli Y were used.

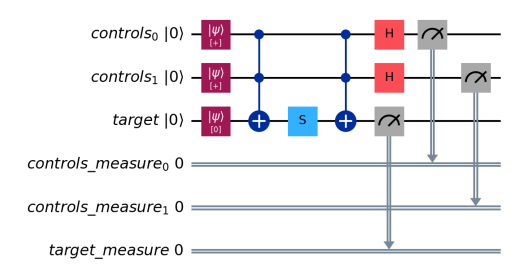


FIG. 9. Circuit implementing $R_{\arccos 3/5}, n=2,3.$

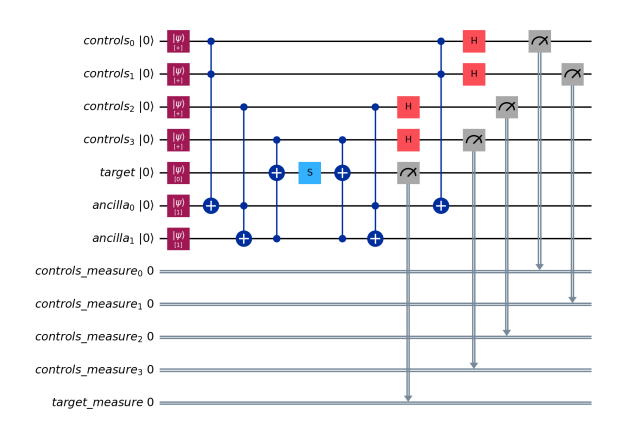


FIG. 10. Single-shot rotation algorithm circuit, n = 4.

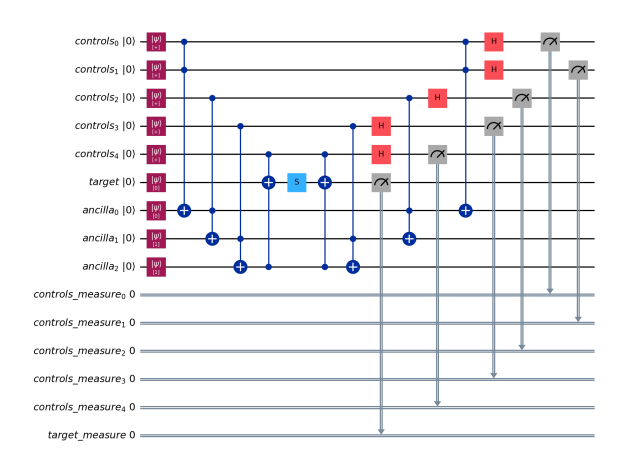


FIG. 11. Single-shot rotation algorithm circuit, n = 5.

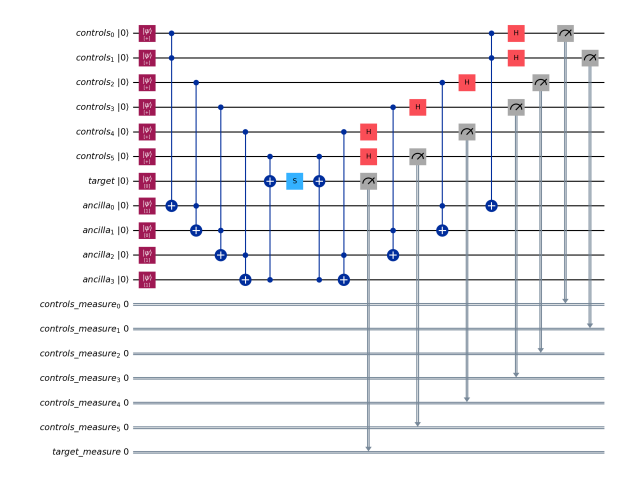


FIG. 12. Single-shot rotation algorithm circuit, n = 6.

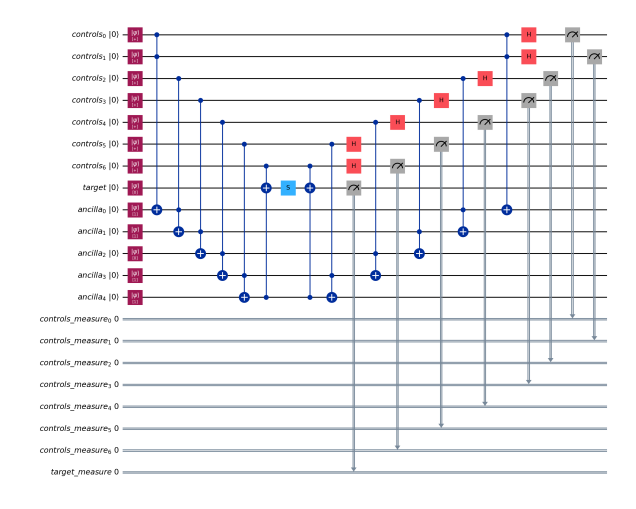


FIG. 13. Single-shot rotation algorithm circuit, n = 7.

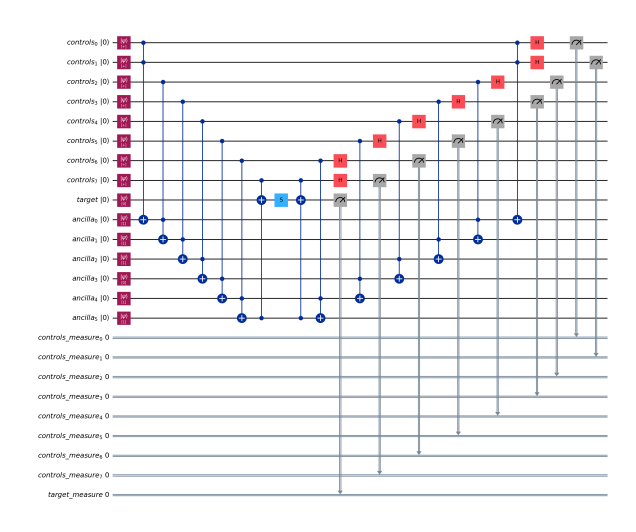


FIG. 14. Single-shot rotation algorithm circuit, n = 8.

Appendix B: Tables

The circuit for n=3 reduces to n=2, so not included below.

n	Prob.			
2	0.62500			
4	0.57031			
5	0.59570			
6	0.58252			
7	0.58899			
8	0.58572			

TABLE I. Theoretical probability of applying T^* .

\overline{n}	δ	Prob.	AGF(T)	PF(T)	AGF(Z)	PF(Z)
2	0.0	0.62485	0.99590	0.99386	1.00038	1.00057
4	0.0	0.57030	1.00035	1.00052	0.99891	0.99837
5	0.0	0.59560	1.00058	1.00086	0.99965	0.99948
6	0.0	0.58278	0.99998	0.99996	1.00209	1.00314
7	0.0	0.58930	0.99992	0.99989	0.99912	0.99868
8	0.0	0.58647	0.99927	0.99891	1.00104	1.00156
2	0.01	0.60219	0.97118	0.95678	0.93977	0.90965
4	0.01	0.52136	0.96942	0.95413	0.90906	0.86358
5	0.01	0.52946	0.97189	0.95783	0.89362	0.84042
6	0.01	0.50276	0.97144	0.95716	0.88114	0.82172
7	0.01	0.49330	0.97431	0.96146	0.86955	0.80433
8	0.01	0.47644	0.97145	0.95717	0.85781	0.78672
2	0.05	0.52658	0.87521	0.81281	0.78282	0.67424
4	0.05	0.37058	0.86807	0.80210	0.73026	0.59538
5	0.05	0.33666	0.87386	0.81079	0.70893	0.56339
6	0.05	0.28466	0.87221	0.80832	0.69726	0.54588
7	0.05	0.25003	0.87209	0.80814	0.68536	0.52805
8	0.05	0.21632	0.87350	0.81024	0.67713	0.51569
2	0.1	0.45124	0.77870	0.66806	0.67766	0.51649
4	0.1	0.25135	0.76845	0.65267	0.64253	0.46379
5	0.1	0.20099	0.77005	0.65507	0.62977	0.44465
6	0.1	0.14947	0.77147	0.65720	0.62468	0.43702
7	0.1	0.11551	0.76797	0.65195	0.62174	0.43261
8	0.1	0.08758	0.77599	0.66398	0.61856	0.42784

TABLE II. Simulated results.

\overline{n}	Err. mit.	Prob.	AGF(T)	PF(T)	AGF(Z)	PF(Z)
2	None	0.37638	0.80831	0.71246	0.74016	0.61024
4	None	0.06921	0.70172	0.55257	0.57163	0.35745
5	None	0.03709	0.54634	0.31952	0.53700	0.30550
6	None	0.01858	0.42861	0.14291	0.53663	0.30495
7	None	0.01668	0.53481	0.30222	0.50642	0.25964
8	None	0.00782	0.47488	0.21232	0.60140	0.40210
2	DD	0.44421	0.86485	0.79728	0.72937	0.59405
4	DD	0.06186	0.64802	0.47203	0.59807	0.39710
5	DD	0.04522	0.63377	0.45066	0.54009	0.31013
6	DD	0.01680	0.61495	0.42243	0.54799	0.32198
7	DD	0.00997	0.55492	0.33237	0.50979	0.26469
8	DD	0.00483	0.51768	0.27652	0.48957	0.23436
2	PT	0.47283	0.87370	0.81055	0.70397	0.55595
4	PT	0.06558	0.50551	0.25826	0.53940	0.30909
5	PT	0.03873	0.55382	0.33073	0.54229	0.31343
6	PT	0.01582	0.59245	0.38868	0.57169	0.35754
7	PT	0.00952	0.50663	0.25995	0.48911	0.23367
8	PT	0.00398	0.49237	0.23855	0.49090	0.23635

TABLE III. Live results. DD stands for dynamical decoupling, and PT for Pauli twirling.